Atmos. Chem. Phys. Discuss., 13, 18581–18620, 2013
www.atmos-chem-phys-discuss.net/13/18581/2013/
doi:10.5194/acpd-13-18581-2013

Atmospheric Chemistry and Physics Discussions
Open Access

Surface response to rain events throughout the West African monsoon

F. Lohou[1], L. Kergoat[2], F. Guichard[3], A. Boone[3], B. Cappelaere[4], J.-M. Cohard[5], J. Demarty[4], S. Galle[5], M. Grippa[2], C. Peugeot[4], D. Ramier[6], C. M. Taylor[7], and F. Timouk[2]

[1]Laboratoire d'Aérologie, UMR5560, Université de Toulouse and CNRS, Toulouse, France
[2]GET (CNRS/UPS/IRD), Toulouse, France
[3]CNRM-GAME (CNRS and Météo-France), Toulouse, France
[4]IRD, Hydrosciences, Montpellier, France
[5]LTHE (UJF), Grenoble, France
[6]CETE Ile de France, Trappes, France
[7]CEH, Wallingford, UK

Received: 24 June 2013 – Accepted: 27 June 2013 – Published: 10 July 2013

Correspondence to: F. Lohou (fabienne.lohou@aero.obs-mip.fr)

Published by Copernicus Publications on behalf of the European Geosciences Union.

Abstract

This study analyses the response of the continental surface to a rain event, taking advantage of the long-term near-surface measurements over different vegetation covers at different latitudes, acquired during the African Monsoon Multidisciplinary Analysis (AMMA) experiment. The simulated surface response by nine land surface models involved in AMMA Land Model Intercomparison Project (ALMIP), is compared to the observations. The surface response, described via the evaporative fraction, evolves in two steps: the immediate surface response and the surface recovery. The immediate surface response corresponds to an increase in the evaporative fraction occurring immediately after the rain. For all the experimental sites, the immediate surface response is strongest when the surface is relatively dry. From the simulation point of view, this relationship is highly model and latitude dependent. The recovery period, characterized by a decrease of the evaporative fraction during several days after the rain, follows an exponential relationship whose rate is vegetation dependent: from 1 day over bare soil to 70 days over the forest. Land surface models correctly simulate the decrease of EF over vegetation covers whereas a slower and more variable EF decrease is simulated over bare soil.

1 Introduction

The monsoon is the main source of precipitation over West-Africa. It generates long-lived mesoscale systems which provide 80 to 90 % of the annual rainfall in the Sahel (D'Amato and Lebel, 1998). Rainfall is characterized by high intermittency and large spatial variability, as well as high temporal variability at the synoptic, intraseasonal, interannual and multidecadal timescales (Lebel et al., 2009; Nicholson, 2013). Land-atmosphere exchanges and surface fluxes are impacted by rainfall variability at all scales, either as a direct response to soil water availability or through vegetation changes, and have been identified as major actors of climate and weather in West-

ACPD
13, 18581–18620, 2013

Africa (Eltahir and Gong, 1996; Zeng et al., 1999; Koster et al., 2004; Taylor et al., 2011b). Recent results demonstrated that convection triggering, which is a critical process in the tropics, was significantly enhanced by mesoscale heterogeneity of surface soil moisture (Taylor et al., 2011a, 2012). Such heterogeneity controls the spatial structure of surface fluxes, with high latent heat flux and low sensible heat flux over the wetted surface whereas the opposite is true over surroundings areas.

The occurrence of these patterns of surface fluxes is linked to rainfall spatial variability and to the size and lifecycle of MCS and squall lines, but it is also related to the way the surface responds to a rain event, which is the focus of the present study. Locally, immediately after a convective rain event, the partitioning of surface fluxes favours the latent heat flux. During the following days, the sensible heat flux progressively increases with the drying of the surface. The surface wetted by a rain event then goes from relatively cold/moist to relatively warm/dry conditions over time, which in turn influences the boundary layer (Schwendike et al., 2010). The temporal dynamics of the latent heat flux after a rain event have been studied in semi-arid regions by Kurc and Small (2004), who highlighted marked differences between grassland and shrubland sites in New Mexico. Focusing on the end-of-season drying for 15 sites worldwide (including sites in Africa), Teuling et al. (2006) pointed out a large variability of drying dynamics, and suggested a prominent importance of vegetation rooting depth. These authors further proposed a possible link between rooting depth and aridity, leading to the observed slower decrease of LE in drier climates. Such behaviour was not successfully simulated by the models involved in the Global Soil Wetness Project 2 which gather offline land surface model runs, compare the LSM schemes and conduct sensitivity studies. A large variability in the land surface model (LSM) response to rain events was also observed by Lohmann and Wood (2003) during the Red-Arkansas PILPS intercomparison exercise, although the absence of measurements prevented pinpointing model errors. Gash et al. (1997) used the HAPEX-Sahel experiment dataset to characterize three land cover types in South-West Niger. Although HAPEX-Sahel was a reference experiment devoted to surface energy balance measurements over the Sahel,

ACPD
13, 18581–18620, 2013

most measurements only focused on the Niamey region, and over a relatively short time period. Altogether, these studies suggest that LSMs might have difficulties in representing flux dynamics in West-Africa. It is also clear that the different land cover types within a region have to be sampled as much as possible, if a reasonable understanding is expected at the regional scale.

The AMMA (African Monsoon Multidisciplinary Analysis) project (Redelsperger et al., 2006) and the AMMA-CATCH observing system (Lebel et al., 2009) were designed to more fully document the multiscale monsoon system over West Africa. Several sites were implemented along a south-north transect providing a rich long-term data set over different vegetation types and climates at different latitudes (Guyot et al., 2009; Ramier et al., 2009; Timouk et al., 2009; Lohou et al., 2010). In parallel, modelling of the land surface during the monsoon was adressed by the AMMA Land Surface Model Intercomparison Project (ALMIP) (Boone et al., 2009). The ALMIP phase 1 scientific objective was to separate the coupling between atmosphere and land surface from the many other couplings (atmospheric, biological) which drive the monsoon system, in order to evaluate LSM sensitivity to atmospheric forcings and intrinsic physics and to develop a climatology of surface diagnostics (Boone et al., 2009). A multimodel offline intercomparison approach used 9 land surface models and their different versions. Even with the same atmospheric forcings, the simulated annual cycle shows a high variability of soil water storage from LSM to LSM (Grippa et al., 2011). This variability partly originates in the accumulation with time of differences occurring during and after each rain event of the monsoon season. Guichard et al. (2010) illustrated the development of such differences in modelled surface fluxes after the occurrence of a large MCS.

Our objectives here are to characterize the dynamics of the surface after a rain event, for a variety of land cover types and climate zones along the S-N transect using observations. A range of LSM are then examined to test their representation of these dynamics, and to diagnose LSM possible weaknesses.

ACPD
13, 18581–18620, 2013

The AMMA experimental surface database and the ALMIP land surface model simulations (Sect. 2) are analysed with the same method both for rain event selection and surface response characterisation (Sect. 3). Whereas the previous studies (Hunt et al., 2002; Kurc and Small, 2004; Teuling et al., 2006) focused on the period after the rain, during which the evapotranspiration decreases, this study takes into account the amplitude of the surface response by comparing the surface fluxes before and after the rain, over the whole year. The decrease of the evaporative fraction with time is modeled by exponential relationships with coefficients that are analysed according to the vegetation cover (Sect. 4.1). The same analysis is carried out with the ALMIP models and the simulated surface response is compared to the experimental one (Sect. 4.2).

2 Data and simulations

Observations from AMMA (African Monsoon and Multidisciplinary Analysis) provide for the first time a continuous data set over several years which characterizes land-surface exchanges and surface properties over West Africa. Several experimental surface sites were deployed along a meridional transect crossing Benin, Niger and Mali and characterising different climatic regimes from humid tropical to sub-saharian regimes. Five of these experimental sites provided throughout several seasonal cycles all the necessary data (surface state and land-atmosphere exchange characteristics) for this study (Fig. 1): forest and fallow in Benin, fallow and millet in Niger and grassland in Mali (hereafter BN-forest, BN-fallow, NG-fallow, NG-millet and ML-grassland, respectively). In addition to the measurements, simulations from 9 Land Surface Models (LSMs) involved in ALMIP where extracted at three locations (hereafter Djougou, Niamey and Hombori locations) encompasing the experimental sites (Fig. 1).

ACPD
13, 18581–18620, 2013

2.1 Flux station sites

The two Benin sites are located in the Donga catchment which is characterized by a typical Sudanian climate. Rainfall is 1200 mm yr^{-1} on average, and potential evapotranspiration is around 1500 mm yr^{-1}. During the monsoon season, from June to October, rainfall events are regular with short dry periods between them (~ 3 days). Before and after the core rainy season (July to September), sparse rainfall occurs during the long transition period from March to May and in November. The climate is well-suited for extensive agricultural practice (30 % of the area) but large areas are still covered with shrub savannah (60 %). Only 10 % of the surface is occupied by scattered forest. Down to 0.5 m depth, the soil is composed of sand and loam. Deeper soil contains also clay that holds water for vegetation. The first flux tower is located on a fallow site surrounded by various crops (Nalohou: 1.6° E, 9.7° N, 449 m). The second is set up over a scattered forest site (Bellefoungou: 1.7° E, 9.8° N, 414 m) where trees are 14 m high on average. These two flux stations are representative of the vegetation density range of this area.

The two Niger sites are located in the Wankama catchment (2.6° E, 13.6° N), typical of the cultivated Sahelian environment of southwest Niger (Cappelaere et al., 2009). The climate is semi-arid tropical with a mean annual rainfall of about 510 mm and a potential evapotranspiration of around 2500 mm yr^{-1} (Favreau et al., 2009). Ninety percent of the rainfall occurs from June to September, mostly from mesoscale convective systems. Soils consist of weakly structured sands and are prone to surface crusting and to erosion. The former natural woody savannah has now been essentially turned into a mosaic of rain-fed millet fields and shrub-covered fallow patches (dominated by *Guiera senegalensis*). The two observation sites sample these two dominant land cover types.

The Mali site is located in the Gourma area, south of the Niger river (1.5° W, 15.5° N). The site is typical of pastoral Sahel, where cropland is scarce (less than 4 % for the so called super-site) (Mougin et al., 2009). Annual precipitation averages 350 mm and falls

ACPD
13, 18581–18620, 2013

between July and mid-September (Frappart et al., 2009). Three main landscape units dominate. The main landscape unit consists of large sandy dunes, with deep soils, covered by annual grasses and scattered trees, which occupy 60 % of the area. Very shallow soils, either rocky outcrops (sandstones, schists) or iron-pans, with very scarce trees, are second in terms of surface, occupying 35 % of the area. Seasonally flooded valleys and ponds, usually densely vegetated, make up the rest of the landscape (5 %). The Agoufou flux tower is set-up on a sandy dune, which is the dominant ecosystem (Timouk et al., 2009).

The surface and atmospheric properties analysed in this study are listed in Table 1. High-frequency measurements were processed with the EdiRe software (Version 1.4.3.1167, R. Clement, University of Edinburgh) on 30 min sample to compute sensible and latent heat flux. CarboEurope recommendations (Mauder and Foken, 2004) were used, including despiking, double rotation, cross-correlation for the derivation of the time lag between the sonic anemometer and the gas analyser, and spectral and Webb corrections. The soil moisture was measured at different depths at each site. It has been vertically integrated over the first meter to ease the comparison between sites and also with the LSMs.

The evolution of the weekly rainfall, and the weekly-averaged leaf area index (LAI), evaporative fraction (EF) and its standard deviation and soil water content at each site are presented in Fig. 2. The evaporative fraction is computed as

$$\mathrm{EF} = \mathrm{LE}/(\mathrm{LE} + H), \quad (1)$$

where LE and H represent the weekly-averaged latent and sensible heat flux, respectively. The measurements were acquired over different periods at each site, between June 2006 and December 2009. One can note the good availability and continuity of the measurements with the exception, in 2009, of the LAI at the Benin sites. These data show the expected south-north gradient of the rainfall and the soil water content. The seasonal evolution of EF is clearly tied to the duration of the monsoon season, with EF reaching similar high values (0.7–0.8) at the different sites, for typically 4 to 5

ACPD
13, 18581–18620, 2013

months in Benin (June to September), 3 to 4 months in Niger (July to September) and 2 months in Mali (July and August).

2.2 Land Surface Model Intercomparison Project

The 9 LSMs used in this study and their ALMIP configuration are summarized in Table 2. In ALMIP phase 1, regional-scale forcing is used. The land surface characteristics for vegetation and soil texture from the ECOCLIMAP database (Masson et al., 2003) were used by all model except HTESSEL and SSiB. The surface meteorology is based on the European Centre for Medium-range Weather Forcast (ECMWF) short-term forecast data and consists of 3 hourly temperature, specific humidity, wind component at 10 m, and surface pressure. For the ALMIP experiment 3 used in this study, the precipitation is from the Tropical Rainfall Measurement Mission (TRMM) precipitation product 3B-42 (Huffman et al., 2007) and the incoming longwave and shortwave fluxes are provided by the LAND-SAF project (Boone et al., 2009). It is important to note that the differences among the simulations shown hereafter can be directly linked to distinct formulations and/or configuration (and surface classification parameters for HTESSEL and SSiB) of the LSMs as they all share the same forcing.

The LSM simulations cover the period 2002 to 2007 with a 0.5° spatial resolution and a 3 h time step. ALMIP data have been extracted at three grid points encompasing the experimental sites in Benin, Mali and Niger. Hereafter these three locations are referred as Djougou, Niamey and Hombori, and the corresponding latitude and longitude coordinates are given in Fig. 1.

The simulated sensible and latent heat fluxes are used to compute the evaporative fraction in the same way as done with the experimental data (Eq. 1). The simulated transpiration (TR) allows an estimation of the vegetation activity. A threshold of 0.1 for transpiration to evapotranspiration ratio (TR / ET) will be used to distinguish bare soil from vegetation cover. The time change of the vertically integrated soil moisture, ΔS, is one of the available variable for soil moisture. S is preferable to a soil moisture-based index since it results from the soil water budget including the precipitation forcing P,

ACPD
13, 18581–18620, 2013

the evapotranspiration ET and the total runoff R:

$$\frac{\partial S}{\partial t} = P - E - R. \quad (2)$$

A time integration of ΔS, simulated with a 3 h time step, defines what will be called hereafter the soil water content anomaly (SWCA) to the 1st of January 2002. SWCA range of variation can be compared from model to model, and to the range of variation of the measured soil moisture. The evolution of the weekly-averaged SWCA, EF and its standard deviation simulated by the 9 LSMs at the three locations are presented in Fig. 3 over the reduced 2005–2006 period for an improved clarity of the figure.

Broadly speaking, EF seasonal evolutions at the three latitudes are well represented by the LSMs with: the higher the latitude, the shorter the period with high EF (4 months in Djougou, 3 months in Niamey and, 2 months in Hombori). However, weekly-averaged EF discrepancy between the LSMs can reach +60 % during the rainy season, and the surface drying at the end of the rainy season is simulated quite differently by the LSMs. Such a discrepancy is also observed in SWCA, with a relative difference of +100 % or more. It would be tempting to link EF and SWCA variability, but the depth of the simulated soil layer varies among LSMs, differences in intercepted water can be important, the water storage in the deep soil is treated differently and runoff varies among LSMs. Therefore, differences in SWCA do not explain differences in EF in a simple way, as already pointed out by Desborough et al. (1996) who compared 13 LSMs simulation of bare soil evaporation.

Although it is not straightforward to compare local measurements to a larger scale simulated pixel, one can remark that ALMIP models simulate a much larger soil water content variation than the observed one. Soil water content at both BN-fallow and BN-forest (Fig. 2) has a 100 mm variation between dry and wet conditions, whereas LSMs give at least a 200 to 300 mm variation (Fig. 3). The same features can be observed at Niger and Mali sites where a 50 to 100 mm variation of soil moisture is measured and a 100 to 200 mm variation is simulated. It is likely that the simulated soil layer depth explain, in part, such a difference.

ACPD
13, 18581–18620, 2013

The standard deviation of EF at the weekly time scale (Figs. 2 and 3) gives clues on the effect of the rain events on the land surface: the larger the EF standard deviation, the higher the effect of the rain events. High standard deviations of about 0.4 (50 % of EF value) can be observed at all sites at the beginning of the monsoon. This impact decreases progressively throughout the rainy season in Benin, lasts longer in Niger, and stays high during the whole monsoon in Mali. Analysis is now conducted by looking at the evolution of the surface fluxes for days either side a rain event.

3 Methods

The same method is applied to select the rain events and quantify the associated surface response to both measured and simulated data.

3.1 Rain event selection

The criteria defined to detect and select a rain event are:

- the rainfall must be preceded by 24 h without rain, which are used to estimate the initial state of the surface.
- the rainfall must be followed by at least 24 h without rain to analyse the surface response. The longer the period without rain the longer the surface recovers from the rain event.
- Only events with cumulated rainfall above 3 mm are selected.
- When two consecutive rainfall events are separated by less than 3 h, they are considered as the same rain event.

According to these criteria, 34 locally-observed events are selected at BN-forest (2008–2009), 50 at BN-fallow (2007–2009), 28 for Niger (2006–2007), and 48 for Mali (2007–2009). The selected ALMIP rain events at each location are the same for all

ACPD
13, 18581–18620, 2013

LSMs since they are driven by the same atmospheric forcings. In 6 yr, 78, 96 and 88 rain events were selected at Djougou, Niamey and Hombori locations, respectively. The rain events in the simulated and measured datasets might not be the same since TRMM rainfall does not always coincide with local measurements, but the statistical analysis of long-term datasets allows a comparison between observed and simulated mean surface responses.

3.2 Surface response

The surface state is considered from the turbulent flux partitioning point of view, via the evaporative fraction. This limits the impact of temporal variability of net radiation on our calculations. H and LE are averaged to get the mean surface response over a 24 h period of time. Only measurements between 06:00 and 18:00 UTC are used to get H and LE means from which EF is computed. $D0$ stands for the 24 h preceding the rainfall, and Dn ($n \geq 1$) stands for the $(n-1) \times 24$ to $n \times 24$ h following the end of the rainfall. As an example, for a rainfall finishing at 15:00 UTC the 22 July, EF at $D1$ stands for the mean evaporative fraction on the 22 July between 15:30 and 18:00 UTC and on the 23 July between 06:00 UTC and 15:00 UTC.

Figure 4 shows an evolution of EF before ($D0$) and after ($D1$ to $D5$) a rain event at NG-fallow. EF at $D0$ gives the initial surface flux partitioning. The rain leads to an increase of EF at $D1$. The ratio EF($D1$) / EF($D0$) depicts the immediate response of the surface. The period following $D1$, during which EF generally decreases with time, is the dry spell during which the surface recovers from the rain event.

The immediate response is of great interest in the context of the African monsoon because it varies a lot along the season according to the soil moisture and vegetation state and defines the initial conditions of the recovery period.

In order to model the surface recovery, Wallace and Holwill (1997) applied a two-stage model on Hapex-Sahel measurements. Evaporation is assumed to occur at its potential rate for 1 day after the rain, then in a second phase, decreases as the square root of time. The surface recovery has also been modeled with a time dependent expo-

ACPD
13, 18581–18620, 2013

nential relationship for: (1) EF decrease after the rain over tussok and rye grasslands in New Zealand by Hunt et al. (2002), and (2) LE (and LE normalized by net radiation and global radiation) decrease over various vegetation covers by Teuling et al. (2006). The evaporative fraction expression reads:

$$\mathrm{EF}(D) = \mathrm{EF}(D1)\exp(-D/\tau_1), \quad (3)$$

where D is time in days after the rainfall and τ_1 is the best fit exponential constant. This model describes the EF decrease from the day after the rainfall (EF($D1$)) until the zero value of EF. Kurc and Small (2004) used the same method to model soil moisture, evapotranspiration and EF over grass and shrub in central New Mexico, but the exponential constant τ_2 is the best fit along a n-day long drydown period which does not necessarily extend to a complete drying of the soil. The evaporative fraction expression is then:

$$\mathrm{EF}(D) = (\mathrm{EF}(D1) - \mathrm{EF}(Dn))\exp(-D/\tau_2) + \mathrm{EF}(Dn). \quad (4)$$

The use of both exponential constants appears to be complementary; the former integrates all the time scales of the successive processes involved in the decrease of EF down to zero; the second gives the time scale of the processes which dominate in the surface drying during the $D1$ to Dn period. In this study, τ_1 and τ_2 are defined as the inverse of the slope of the linear regression of $\ln(\mathrm{EF}(D)/\mathrm{EF}(D1))$ and $\ln((\mathrm{EF}(D) - \mathrm{EF}(Dn))/(\mathrm{EF}(D1) - \mathrm{EF}(Dn)))$ with time, respectively. τ_1 and τ_2 are determined for the median surface response computed over the selected rain events whose recovery period are at least 5 days long. The 5 day recovery period is a compromise between the longest possible period to correctly represent the surface evolution throughout its drying and the highest number of rain events used to compute the median surface response. τ_1 and τ_2 uncertainties are computed as the slope uncertainties.

ACPD
13, 18581–18620, 2013

4 Results

4.1 Observed surface response to a rain event

4.1.1 Immediate surface response

Several surface and atmospheric properties can drive the amplitude of the immediate surface response (EF($D1$)/EF($D0$)): soil water content, vegetation and its root layer depth, rainfall, potential evapotranspiration... Among them, the soil water content, because of its strong seasonal variation, is expected to dominate the evolution of EF($D1$)/EF($D0$) throughout the monsoon. Actually, before the core of the rainy season, the surface soil water content is close to the wilting point value, so that the first rainfall events change significantly the surface humidity and then lead to a strong increase of the evaporative fraction. In contrast, the evaporative fraction of a soil whose surface water content is already close to its field capacity value should not vary a lot after a rain event. These cases are very frequent in Benin but much less frequent in Mali even at the end of the rainy season as shown by EF standard deviation in Figs. 2 and 3.

The sensitivity of the immediate surface response to soil water content before the rain is shown in Fig. 5. Soil moisture varies among sites according to (1) the latitude, (2) the soil texture and (3) the vegetation type. The extreme values are measured for the BN-forest (200 to 300 mm) and for the ML-grassland (0 to 60 mm). This shift aside, a similar behaviour is found for all the sites: the lower the soil water content, the higher the immediate surface response. These high immediate surface responses mainly occur at the beginning of the monsoon when the LAI is close to zero (not shown) and then when the vegetation activity is still very low (except for BN-forest site where the vegetation is almost evergreen). Consequently these high immediate responses are much more related to soil evaporation than transpiration. A distinction between smaller and larger rainfall than an arbitrary threshold of 8 mm (Fig. 5) shows that the immediate response does not depend on the cumulated precipitation when it is above 3 mm. Lastly, no clear relationship has been pointed out between the potential evapotranspiration and the

ACPD
13, 18581–18620, 2013

immediate response, meaning that atmospheric demand is never limiting enough in these regions for these high immediate response events (not shown).

4.1.2 Surface recovery

As expected, the seasonal cycle of surface recovery is close to the cycle of the immediate response. Figure 6 illustrates the strong link between the immediate surface response (EF($D1$)/EF($D0$)) and surface recovery amplitude on $D2$ (EF($D1$)/EF($D2$)). This power relationship shows a strong coherence between the way the surface reacts just after the rain and the way it recovers on $D2$, whatever the site. During the early monsoon, the EF increase on $D1$ is mainly due to bare soil and interception evaporation which weakens on $D2$, implying a decrease of EF. Later in the season, both surface response and surface recovery amplitudes tend toward one when soil moisture is not highly affected by the rain and/or transpiration takes over evaporation.

Figure 7 gathers EF evolution with time for all the rainfall events selected at each site. EF is normalised by EF($D1$) for more clarity. The rain events are further sorted in two categories according to the LAI. LAI above 0.01 corresponds to a vegetation coverage, whereas LAI below 0.01 represents a bare soil. All of the sites (but those in Benin) provide both bare soil (at the beginning of the monsoon) and vegetated surface (during the monsoon) recovery.

EF median evolution with time is computed up to $D5$ for the vegetation and bare soil cases, using only rain events whose following dry period lasts at least 5 days. Values of τ_1 and τ_2 and their uncertainties are presented in Table 3.

For bare soil, both τ_1 and τ_2 have low values: $\tau_1 \sim 1.3$–2.9 days and $\tau_2 \sim 1$ day. For vegetation covers, τ_1 and τ_2 are larger than for bare soil because the transpiration process is added to the evaporation and slows the decrease of EF. Without quantifying it, Dugas et al. (1996) already observed such a difference over arid surfaces of the south-western United States. τ_2 ranges from 1.7 to 5.5 days and is to be compared to 2 days found by Kurc and Small (2004). τ_1 for vegetation covers is above 6 days, as found by Hunt et al. (2002), and corresponds to different rooting systems and rooting

ACPD
13, 18581–18620, 2013

depth. The deeper the roots, the longer τ_1, with 7 to 10 days for annual vegetation as grass and millet, 10 to 21 days for fallow with shrubs and 74 days for the forest. As mentioned by Teuling et al. (2006), τ seems to have a stronger relation with vegetation type than with soil type.

Uncertainties are generally lower than 10 %, except for NG-fallow where it is about 20 %, and for BN-forest where it reaches about 75 %. The latter can be explained by the use of only two rain events with a 5 day long recovery period but also because the recovery period is two short for this type of vegetation covers. However, τ_1 of 74 days is coherent with values found by Teuling et al. (2006) for forest sites.

4.2 Simulated surface response to a rain event

The two stages of EF evolution, immediate response and surface recovery, are analysed with the same method used for the experiment. However, one must keep in mind the difference of horizontal resolution (less than 1 km footprint for the experiment, and 0.5° square for the ALMIP models) and also the larger statistical sample for the models (2 to 3 yr for the experiment and 6 yr for the ALMIP models).

4.2.1 Immediate surface response

The immediate surface response as a function of soil moisture is illustrated for 3 of the 9 LSMs in Fig. 8 for Djougou, Niamey and Hombori locations. The three simulations have been chosen to represent the diversity of the simulated surface response.

Whilst the relationship between immediate response and soil water content is similar from site to site in the experiment (Fig. 5), it can be very different between the LSMs at a given location, and also, between locations for a given LSM. For Djougou, the LSMs are quite in agreement since the surface and vegetation respond in any case very little to rain events, the soil being sufficiently moist or the roots deep enough. The differences increase for drier soils at higher latitudes where the evaporative fraction turns out to be very sensitive to evaporation and transpiration schemes. Schüttemeyer

ACPD
13, 18581–18620, 2013

et al. (2008) already pointed out the various sensitivities of simulated surface fluxes to soil moisture comparing HTESSEL and NOAH. At Niamey, the relationship between the surface response and SWCA continously varies from an almost linear relationship, as in Fig. 8d and f, to a binary relationship for which the surface does not respond unless SWCA is zero, like in Fig. 8e (the intermediate relationships are not shown). At the drier location of Hombori, most of the LSMs tend to loose the relationship between immediate reponse and SWCA.

In addition, the simulated immediate response is slightly overestimated (0 to 3 times) most of the time at Djougou and Niamey, and it is highly overestimated (3 to 10 times) at Hombori, compared to the experiment (Fig. 8).

4.2.2 Surface recovery

The relationship between the immediate surface response and the amplitude of EF recovery are quite differently simulated by the LSMs. Whereas the relationship in Fig. 9a is similar to the exprimental one, the LSM in Fig. 9b tends to simulate a high evaporative fraction on $D2$ with many cases where EF($D2$) $\approx$ EF($D1$). This means that a strong increase of EF on $D1$ is not followed by a drecrease of EF on $D2$ as it has been generally observed (Fig. 6). On the contrary, the LSM in Fig. 9c tends to simulate a large decrease of EF on $D2$ compared to the increase on $D1$. The model whose results are close to the observed empirical relationship (Fig. 9a) is also the one whose simulated immediate response is clearly linked to SWCA (Fig. 8a, d, g).

The median of the simulated EF/EF($D1$) evolution after the rain events selected during 6 monsoon seasons, are estimated considering vegetation covers (TR / ET $\geq$ 0.1) and bare soil (TR / ET $<$ 0.1) (Fig. 10 left and middle panels). Some LSMs (CLSM, HTESSEL) have no rain events over bare soil at Djougou, and in contrast, some LSMs (SSiB, SWAP) have no rain events over vegetation cover at Hombori. As already observed for the experimental results, the decrease of EF between two rain events is more rapid over bare soil than over vegetation cover.

ACPD
13, 18581–18620, 2013

There is a relatively good agreement between models for vegetation covers, despite the differences between the simulated median evolution of the partitioning evapotranspiration/evaporation (Fig. 10, right panels). The time evolution of TR / ET ratio shows that evaporation turns to be the main contribution to the simulated surface latent heat flux right after the rain (at $D1$), and then it gradually decreases. For HTESSEL, transpiration is largely overriding, and nonetheless, the surface recovery is correctly simulated.

Estimates of τ_1 and τ_2 for the experiment and the simulated data are gathered in Fig. 11. For bare soils, τ_1 and τ_2 values deduced from experimental data are below 3 days (Table 3), whatever the soil type and the latitude. The values deduced from simulated data varies between 1 and 8 days. The standard deviation of these estimates varies between 0.5 and 1.9 days as a function of the site (Fig. 11). It represents a discrepancy between LSMs of 25 to 50 % of the mean value of τ, which is not negligible considering that τ_1 and τ_2 accuracy is less than 10 % for most of the LSMs (not shown).

The experimental values of τ_1 at each location reflect the vegetation diversity which decrease with increasing latitude. Actually, at Djougou, other vegetation covers could have been studied, in particular cultivated fields (crops, . . .). In Niamey, the two surface stations sampled the two dominant land cover types. In Hombori, the sampled grassland represents 60 % of the landscape and 92 % of the vegetated surface (densely vegetated surface during the monsoon season occupying 5 % of the area is not taken into account in this study, Timouk et al., 2009). Vegetation and soil texture in the LSMs are defined by ECOCLIMAP database (but for HTESSEL and SSiB) and the simulated EF presented in this study is an average over the grid point. Simulated τ_1 is then expected to be a weighted average of the experimental ones.

The simulated τ_1 variability from LSM to LSM is about 25 % at Niamey and Hombori. Then the spread across LSMs appear to be more important for bare soil conditions (25 to 50 %) than for vegetation covers. As seen previously, the limit of the method is reached for Djougou, where the 5 day recovery period is too short to accuratly estimate a large exponential coefficient.

ACPD
13, 18581–18620, 2013

5 Discussion

Several empirical relationships have been derived from the AMMA surface measurements to better describe and understand the way the land surface responds to a rain event in a large range of surface caracteristics (soil moisture, vegetation types). It is interesting to note the consistency of the experimental results from one site to the other, along the meridional transect. It has been shown that the relationships are simulated quite differently by the LSMs.

The simulated immediate response of the surface, i.e. the increase in EF the day after the rain, is not as clearly linked to soil moisture (Fig. 8) as it is in the observations (Fig. 6). Furthermore, most of the LSMs tend to overestimate the EF increase after the rain, particularly at the highest latitude. Because the EF increase in $D1$ is mainly due to an increase in evaporation, several reasons could explain this overestimation by the LSMs, as an excess of interception or a limited drainage. However, it is questionable whether an over or under estimation of some processes, such as drainage or interception, can lead to a loss of relationship between surface response and soil moisture, in particular for small LAI. Modeling bare soil evaporation is still an issue for LSM.

The exponential decrease of EF during the dry period over bare soil is modeled with larger exponential coefficients in the simulation than in the experiment (Fig. 11). This means that, on average, the decrease of EF over bare soil is slower in the simulations. On the other hand, over vegetation covers, simulated and experimental exponential coefficients are in the same range. Then differences between surface responses over bare soils and vegetations covers might be weaker in the simulations than they are in reality. This would lead to weaker surface heterogeneities whose role are important in convection initiation.

The dispersion of the exponential coefficient values among LSMs shows how the different schemes can speed or slow EF decrease throughout the dry period. The dispersion is particularly important in two cases: (1) over bare soil and (2) over grid points encompassing different vegetation types.

ACPD
13, 18581–18620, 2013

Several Evaporation formulations have been compared by Mahfouf and Noilhan (1991) who pointed out a clear overestimation of nighttime evaporation with bulk aerodynamic formulations whereas threeshold formulations are highly sensitive to the depth of the surface layer.

As in Teuling et al. (2006), the rooting depth is found to strongly influence the flux recovery after a rain event. However, the more arid sites do not have the larger rooting depth. In fact, the dominant driver is the phenology of the dominant plants, with perennial plants found in forest and fallows (and tiger bush systems, not sampled here but common in some parts of the Sahel), and less so in annual-dominated ecosystemes like Sahelian grasslands and croplands. Note that trees and bushes are found in arid Sahel, but usually at low density. A proper representation of the annual/perennial types of plants is therefore very important for simulating surface/atmosphere exchanges in West Africa.

These disparities between the simulated and the experimental relationships for the surface response and surface recovery do not necessarily explain model dispersion at the annual time scale. It is difficult to know whether the errors are cumulative or whether they balance each other. The immediate response of the surface defines the initial conditions of the recovery period. Then, an overestimation of the simulated immediate response could shift the evaporative fraction toward high values during the whole dry period. On the contrary, this overestimation of the surface response after the rain could also be balanced by an unusually weak exponential coefficent leading to a faster decrease of EF during the following days.

6 Conclusions

Several years of surface–atmosphere exchange measurements, over different vegetation covers, at different latitudes in West Africa were acquired during the AMMA experiment. The measured evaporative fraction, soil moisture and leaf area index give a good description of the evolution of the surface and the energy flux partitioning after

ACPD
13, 18581–18620, 2013

a rain event, throughout the monsoon, over bare soil and vegetation covers (fallow and forest in Benin, fallow and millet in Niger and grassland in Mali). In complement to the AMMA experiment, the ALMIP project provides several years of land surface model simulations.

In this study, the surface response is split into two stages: (1) the immediate surface response which corresponds to evaporative fraction increase right after the rain and (2) the surface recovery period during which the evaporative fraction decreases with time.

The measurements analysis shows that the soil water content before the rain mainly determines the amplitude of the surface immediate response: the lower the soil moisture, the higher the surface immediate response. Large surface responses are then observed at the beginning of the monsoon when the soil moisture is still close to its wilting point value. The relationship between immediate surface response and soil moisture in the experiment is very similar from sites to sites, independent of the latitude. This is not the case in the simulations. The relationship, when it exists, is LSM and latitude dependent. Furthermore, the increase in EF after the rain tends to be overestimated by the LSMs.

The decrease of the experimental evaporative fraction during the dry period is modeled by two exponential relationships previously used by Hunt et al. (2002); Kurc and Small (2004) and Teuling et al. (2006). Evaporative fraction over bare soil has been shown to decrease with a 1.0–2.9 day exponential coefficient at both the Niger and Mali sites. The exponential coefficients for vegetation covers are higher and depend on the root depth, varying between 7 days for the grassland and 74 days for the forest. The phenology of the dominant plants proved to be critical for the surface recovery, in particuliar the density of perenial plants (shrubs, trees). In the simulations, the decrease in EF over bare soil is less well simulated than over vegetation covers, with an overestimation and a high discrepancy of the exponential coefficient.

The detailed study of the way the surface responds to a rain event over the West African continent points out some LSM weaknesses which, integrated over the whole monsoon season, may help explain the annual variability among LSMs. The bare soil

ACPD
13, 18581–18620, 2013

evaporation appears to be one of these weaknesses which leads to a lack of relationship between surface response and soil moisture and to a LSMs disparity during the recovery period.

Acknowledgements. This work was supported by the AMMA project. AMMA was built by an international scientific group and was funded by a large number of agencies, especially from France, UK, US and Africa. Field data were collected by the Service d'Observation AMMA-CATCH (www.amma-catch.org).

The publication of this article is financed by CNRS-INSU.

References

Balsamo, G., Viterbo, P. A., Beljaars, A., van den Hurk, B., Hirschi, M., Betts, A. K., and Scipal, K.: A revised hydrology for the ecmwf model: verification from field site to terrestrial water storage and impact in the integrated forecast system, J. Hydrometeorol., 10, 623–643, doi:10.1175/2008JHM1068.1, 2009. 18608

Boone, A., Masson, V., Meyers, T., and Noilhan, J.: The influence of the inclusion of soil freezing on simulations by a soil–vegetation–atmosphere transfer scheme, J. Appl. Meteorol., 39, 1544–1569, 2000. 18608

Boone, A., De Rosnay, P., Balsamo, G., Beljaars, A., Chopin, F., Decharme, B., Ducharne, A., Gascoin, S., Grippa, M., Guichard, F., Gusev, Y., Harris, P., Jarlan, L., Kergoat, L., Mougin, E., Nasonova, O., Norgaard, A., Orgeval, T., Ottlé, C., Poccard-Leclerc, I., Polcher, J., Sandholt, I., Saux-Picard, S., Taylor, C., and Xue, Y.: The AMMA LAnd SurfAce ModeL inTercoMpAriSon projecT (ALMip), B. Am. Meteorol. Soc., 39, 1865–1880, doi:10.1175/2009BAMS2786.1, 2009. 18584, 18588

Boulain, N., Cappelaere, B., Ramier, D., Issoufou, H. B. A., Halilou, O., Seghieri, J., Guillemin, F., Oï, M., Gignoux, J., and Timouk, F.: Towards an understanding of coupled

ACPD
13, 18581–18620, 2013

physical and biological processes in the cultivated Sahel – 2. Vegetation and carbon dynamics, J. Hydrol., 375, 190–203, doi:10.1016/j.jhydrol.2008.11.045, 2009. 18607
Cappelaere, B., Descroix, L., Lebel, T., Boulain, N., Ramier, D., Laurent, J., Favreau, G., Boubkraoui, S., Boucher, M., Moussa, I. B., Chaffard, V., Hiernaux, P., Issoufou, H. B. A., Breton, E. L., Mamadou, I., Nazoumou, Y., Oi, M., Ottlé, C., and Quantin, G.: The AMMA-CATCH experiment in the cultivated Sahelian area of south-west Niger – investigating water cycle response to a fluctuating climate and changing environment, J. Hydrol., 375, 34–51, doi:10.1016/j.jhydrol.2009.06.021, 2009. 18586
D'Amato, N. and Lebel, T.: On the characteristics of the rainfall events in the sahel with a view to the analysis of climatic variability, Int. J. Climatol., 18, 955–974, 1998. 18582
Decharme, B.: Influence of runoff parameterization on continental hydrology: comparison between the Noah and the ISBA land surface models, J. Geophys. Res., 112, D19108, doi:10.1029/2007JD008463, 2007. 18608
de Rosnay, P., Gruhier, C., Timouk, F., Baup, F., Mougin, E., Hiernaux, P., Kergoat, L., and LeDantec, V.: Multi-scale soil moisture measurements at the Gourma meso-scale site in Mali, J. Hydrol., 375, 241–252, doi:10.1016/j.jhydrol.2009.01.015, 2009. 18607
Desborough, C. E., Pitman, A. J., and Irannejad, P.: Analysis of the relationship between bare soil evaporation and soil moisture simulated by 13 land surface schemes for a simple non-vegetated site, Global Planet. Change, 13, 47–56, 1996. 18589
d'Orgeval, T., Polcher, J., and de Rosnay, P.: Sensitivity of the West African hydrological cycle in ORCHIDEE to infiltration processes, Hydrol. Earth Syst. Sci., 12, 1387–1401, doi:10.5194/hess-12-1387-2008, 2008. 18608
Dugas, W. A., Hicks, R. A., and Gibbens, R. P.: Structure and function of C 3 and C 4 Chihuahuan Desert plant communities. Energy balance components, J. Arid Env., 34, 63–79, 1996. 18594
Eltahir, E. A. B. and Gong, C.: Dynamics of wet and dry years in West Africa, J. Climate, 9, 1030–1042, 1996. 18583
Essery, R. L. H., Best, M. L., Betts, A. K., Cox, P. M., and Taylor, C. M.: Explicit representation of subgrid heterogeneity in a GCM land surface scheme, J. Hydrometeorol., 4, 530–543, 2003. 18608
Favreau, G., Cappelaere, B., Massuel, S., Leblanc, M., Boucher, M., Boulain, N., and Leduc, C.: Land clearing, climate variability, and water resources increase in semiarid southwest Niger: a review, Water Resour. Res., 45, 1–18, doi:10.1029/2007WR006785, 2009. 18586

ACPD
13, 18581–18620, 2013

Frappart, F., Hiernaux, P., Guichard, F., Mougin, E., Kergoat, L., Arjounin, M., Lavenu, F., Koité, M., Paturel, J.-E., and Lebel, T.: Rainfall regime across the Sahel band in the Gourma region, Mali, J. Hydrol., 375, 128–142, doi:10.1016/j.jhydrol.2009.03.007, 2009. 18587, 18607

Gash, J., Kabat, P., Monteny, B., Amadou, M., Bessemoulin, P., Billing, H., Blyth, E., DeBruin, H. A. R., Elbers, J., Friborg, T., Harrison, G., Holwill, C., Lloyd, C., Lhomme, J.-P., Moncrieff, J., Puech, D., Soegaard, H., Taupin, J., Tuzet, A., and Verhoeff, A.: The variability of evaporation during the HAPEX-Sahel Intensive Observation Period, J. Hydrol., 189, 385–399, 1997. 18583

Grippa, M., Kergoat, L., Frappart, F., Araud, Q., Boone, A., de Rosnay, P. J.-M, L., Gascoin, S., Balsamo, G., Ottlé, C., Decharme, B., Saux-Picart, S., and Ramillien, G.: Land water storage variability over West Africa estimated by Gravity Recovery and Climate Experiment (GRACE) and land surface models, Water Resour. Res., 47, 1–18, doi:10.1029/2009WR008856, 2011. 18584

Guichard, F., Asencio, N., Peugeot, C., Bock, O., Redelsperger, J.-L., Cui, X., Garvert, M., Lamptey, B., Orlandi, E., Sander, J., Fierli, F., Gaertner, M. A., Jones, S. C., Lafore, J.-P., Morse, A., Nuret, M., Boone, A., Balsamo, G., de Rosnay, P., Decharme, B., Harris, P. P., and Bergès, J.-C.: An intercomparison of simulated rainfall and evapotranspiration associated with a mesoscale convective system over West Africa, Weather Forecast., 25, 37–60, doi:10.1175/2009WAF2222250.1, 2010. 18584

Gusev, E. M., Nasonova, O. N., and Kovalev, E. E.: Modeling the components of heat and water balance for the land surface of the globe, Water Resour., 33, 616–627, 2006. 18608

Guyot, A., Cohard, J.-M., Anquetin, S., Galle, S., and Lloyd, C. R.: Combined analysis of energy and water balances to estimate latent heat flux of a sudanian small catchment, J. Hydrol., 375, 227–240, doi:10.1016/j.jhydrol.2008.12.027, 2009. 18584

Huffman, G. J., Adler, R. F., Bolvin, D. T., Gu, G., Nelkin, E. J., Bowman, K. P., Hong, Y., Stocker, E. F., and Wolff, D. B.: The TRMM Multisatellite Precipitation Analysis (TMPA): quasi-global, multiyear, combined-sensor precipitation estimates at fine scales, J. Hydrometeorol., 8, 38–55, doi:10.1175/JHM560.1, 2007. 18588

Hunt, J., Kelliher, F., McSeveny, T., and Byers, J.: Evaporation and carbon dioxide exchange between the atmosphere and a tussock grassland during a summer drought, Agr. Forest Meteorol., 111, 65–82, doi:10.1016/S0168-1923(02)00006-0, 2002. 18585, 18592, 18594, 18600

ACPD
13, 18581–18620, 2013

Koster, R. D., Suarez, M. J., Ducharne, A., Stieglitz, M., and Kumar, P.: A catchment-based approach to modeling land surface, J. Geophys. Res., 105, 24809–24822, 2000. 18608
Koster, R. D., Dirmeyer, P. A., Guo, Z., Bonan, G., Chan, E., Cox, P., Gordon, C. T., Kanae, S., Kowalczyk, E., Lawrence, D., Liu, P., Lu, C.-H., Malyshev, S., McAvaney, B., Mitchell, K., Mocko, D., Oki, T., Oleson, K., Pitman, A., Sud, Y. C., Taylor, C. M., Verseghy, D., Vasic, R., Xue, Y., and Yamada, T.: Regions of strong coupling between soil moisture and precipitation, Science, 305, 1138–1140, doi:10.1126/science.1100217, 2004. 18583
Kurc, S. A. and Small, E. E.: Dynamics of evapotranspiration in semiarid grassland and shrubland ecosystems during the summer monsoon season, central New Mexico, Water Resour. Res., 40, 1–15, doi:10.1029/2004WR003068, 2004. 18583, 18585, 18592, 18594, 18600
Lebel, T., Cappelaere, B., Galle, S., Hanan, N., Kergoat, L., Levis, S., Vieux, B., Descroix, L., Gosset, M., Mougin, E., Peugeot, C., and Seguis, L.: AMMA-CATCH studies in the Sahelian region of West-Africa: an overview, J. Hydrol., 375, 3–13, doi:10.1016/j.jhydrol.2009.03.020, 2009. 18582, 18584
Lohmann, D. and Wood, E. F.: Timescales of land surface evapotranspiration response in the PILPS phase 2(c), Global Planet. Change, 38, 81–91, doi:10.1016/S0921-8181(03)00007-9, 2003. 18583
Lohou, F., Saïd, F., Lothon, M., Durand, P., and Serça, D.: Impact of boundary-layer processes on near-surface turbulence within the West African Monsoon, Bound.-Lay. Meteorol., 136, 1–23, doi:10.1007/s10546-010-9493-0, 2010. 18584
Mahfouf, J.-F. and Noilhan, J.: Comparative Study of Various Formulations of Evaporation from Bare Soil Using In Situ Data, J. Appl. Meteorol., 30, 1354–1365, 1991. 18599
Masson, V., Champeaux, J., Chauvin, F., Meriguet, C., and Lacaze, R.: A global database of land surface parameters at 1-km resolution in meteorological and climate models, J. Climate, 16, 1261–1282, 2003. 18588
Mauder, M. and Foken, T.: Documentation and Instruction Manual of the Eddy Covariance Software Package TK2, Work Report University of Bayreuth, Dept. of Micrometeorology, ISSN 1614-8916, 26, 42 pp., available at: http://opus.ub.uni-bayreuth.de/volltexte/2011/800/, 2004. 18587
Mougin, E., Hiernaux, P., Kergoat, L., Grippa, M., Rosnay, P. D., Timouk, F., Dantec, V. L., Demarez, V., Lavenu, F., Arjounin, M., Lebel, T., Soumaguel, N., Ceschia, E., Mougenot, B., Baup, F., Frappart, F., Frison, P. L., Gardelle, J., Gruhier, C., Jarlan, L., Mangiarotti, S., Sanou, B., Tracol, Y., Guichard, F., Trichon, V., Diarra, L., Soumaré, A., Koité, M., Dembélé, F.,

ACPD
13, 18581–18620, 2013

Lloyd, C., Hanan, N. P., Damesin, C., Delon, C., Serça, D., Seghieri, J., Becerra, S., Dia, H., Gangneron, F., and Mazzega, P.: The AMMA-CATCH Gourma observatory site in Mali: relating climatic variations to changes in vegetation, surface hydrology, fluxes and natural resources, J. Hydrol., 375, 14–33, doi:10.1016/j.jhydrol.2009.06.045, 2009. 18586, 18607

Nicholson, S. E.: The West African Sahel: a review of recent studies on the rainfall regime and its interannual variability, ISRN Meteorology, 2013, 1–32, doi:10.1155/2013/453521, 2013. 18582

Ramier, D., Boulain, N., Cappelaere, B., Timouk, F., Rabanit, M., Lloyd, C. R., Boubkraoui, S., Métayer, F., Descroix, L., and Wawrzyniak, V.: Towards an understanding of coupled physical and biological processes in the cultivated Sahel – 1. Energy and water, J. Hydrol., 375, 204–216, doi:10.1016/j.jhydrol.2008.12.002, 2009. 18584, 18607

Redelsperger, J.-L., Thorncroft, C. D., Diedhiou, A., Lebel, T., Parker, D. J., and Polcher, J.: African monsoon multidisciplinary analysis, B. Am. Meteorol. Soc., 87, 1739–1746, doi:10.1175/BAMS-87-12-1739, 2006. 18584

Saux-Picart, S., Ottlé, C., Decharme, B., André, C., Zribi, M., Perrier, A., Coudert, B., Boulain, N., Cappelaere, B., Descroix, L., and Ramier, D.: Water and energy budgets simulation over the AMMA-Niger super-site spatially constrained with remote sensing data, J. Hydrol., 375, 287–295, doi:10.1016/j.jhydrol.2008.12.023, 2009. 18608

Schüttemeyer, D., Moene, A. F., Holtslag, A. A. M., and de Bruin, H. A. R.: Evaluation of two land surface schemes used in terrains of increasing aridity in West Africa, J. Hydrometeorol., 9, 173–193, doi:10.1175/2007JHM797.1, 2008. 18595

Schwendike, J., Kalthoff, N., and Kohler, M.: The impact of mesoscale convective systems on the surface and boundary-layer structure in West Africa: case-studies from the AMMA campaign 2006, Q. J. Roy. Meteor. Soc., 136, 566–582, doi:10.1002/qj.599, 2010. 18583

Taylor, C. M., Gounou, A., Guichard, F., Harris, P. P., Ellis, R. J., Couvreux, F., and Kauwe, M. D.: Frequency of Sahelian storm initiation enhanced over mesoscale soil-moisture patterns, Nat. Geosci., 4, 430–433, doi:10.1038/ngeo1173, 2011a. 18583

Taylor, C. M., Parker, D. J., Kalthoff, N., Gaertner, M. A., Philippon, N., Bastin, S., Harris, P. P., Boone, A., Agusti-Panareda, A., Baldi, M., Cerlini, P., Descroix, L., Flamant, C., Grandpeix, J.-Y., and Polcher, J.: New perspectives on land–atmosphere feedbacks from the African Monsoon Multidisciplinary Analysis, Atmos. Sci. Lett., 44, 38–44, doi:10.1002/asl.336, 2011b. 18583

ACPD
13, 18581–18620, 2013

Taylor, C. M., de Jeu, R. A. M., Guichard, F., Harris, P. P., and Dorigo, W. A.: Afternoon rain more likely over drier soils, Nature, 489, 423–426, doi:10.1038/nature11377, 2012. 18583

Teuling, A. J., Seneviratne, S. I., Williams, C., and Troch, P. A.: Observed timescales of evapotranspiration response to soil moisture, Geophys. Res. Lett., 33, L23403, doi:10.1029/2006GL028178, 2006. 18583, 18585, 18592, 18595, 18599, 18600

Timouk, F., Kergoat, L., Mougin, E., Lloyd, C., Ceschia, E., Cohard, J.-M., Rosnay, P. D., Hiernaux, P., Demarez, V., and Taylor, C.: Response of surface energy balance to water regime and vegetation development in a Sahelian landscape, J. Hydrol., 375, 178–189, doi:10.1016/j.jhydrol.2009.04.022, 2009. 18584, 18587, 18597, 18607

Wallace, J. and Holwill, C.: Soil evaporation from tiger-bush in south-west Niger, J. Hydrol., 188–189, 426–442, doi:10.1016/S0022-1694(96)03185-X, 1997. 18591

Xue, Y., Sellers, P. J., Kinter, J., and Shukla, J.: A simplified Biosphere Model for Global Climate Studies, J. Climate, 4, 345–364, 1991. 18608

Zeng, N., Neelin, J. D., Lau, K.-M., and Tucker, J.: Enhancement of interdecadal climate variability in the sahel by vegetation interaction, Science, 286, 1537–1540, doi:10.1126/science.286.5444.1537, 1999. 18583

ACPD
13, 18581–18620, 2013

Table 1. Variables and associated instrument used at the experimental sites.

Variable	Instrument	reference
Rainfall	0.5 mm resolution tipping bucket raingauge	Frappart et al. (2009)
Leaf area index	photographs analyzed with CAN-EYE software leaves collection along a 1 km transect	Boulain et al. (2009) Mougin et al. (2009)
Soil moisture	CS616 capacity probes (Campbell Sci. Inc) at 0.05, 0.1, 0.2, 0.4, 0.6 and 1 m-depths at Benin sites at 0.1, 0.5 and 1.0 m-depths at Niger sites at 0.05, 0.1, 0.4, 1.2, 2.2 m-depths at Mali site	Ramier et al. (2009) de Rosnay et al. (2009)
Sensible and Latent Heat flux	Cstat-3 20-Hz sonic anemometer (Campbell Sci. Inc) and Li7500 infrared gas at 5 (BN-fallow), 18 (BN-forest), 5 (NG-fallow and NG-millet) and 3.5 (ML-grassland) m-heights	Ramier et al. (2009) Timouk et al. (2009)
Radiation flux	Kipp & Zonen CNR1 Radiometer	Timouk et al. (2009)

ACPD
13, 18581–18620, 2013

Table 2. Land Surface model participating in ALMIP experiment 3. The model configuration used for ALMIP is summarized in the last column with the number of vertical soil layers (L), number of energy budgets E per tile, and the soil-vegetation parameters used (SV). Tile refers to the maximum number of completely independent land surface types permitted within each grid box.

Model acronym	Institute Recent reference	ALMIP configuration
HTESSEL	ECMWF, UK Balsamo et al. (2009)	4L, 6 tiles, 1E SV: ECMWF
ORCHIDEE_CWRR	IPSL, France D'Orgeval et al. (2008)	11L, 13 tiles, 1E SV: Ecoclimap
ISBA_DF	CNRM, France Boone et al. (2000)	5L, 1 tile, 1E SV: Ecoclimap
JULES	CEH, UK Essery et al. (2003)	4L, 9 tiles, 1E SV: Ecoclimap
SETHYS	CETP, France Saux-Picart et al. (2009)	2L, 12 tiles, 2E SV: Ecoclimap
NOAH	CETP/LSCE(NCEP) Decharme (2007)	7L, 12 tiles, 1E SV: Ecoclimap
CLSM	UPMC, France Koster et al. (2000)	3L, 5 tiles, 1E SV: Ecoclimap
SSiB	LETG, France Xue et al. (1991)	3L, 1 tile, 2E SV: SSiB
SWAP	IWP, Russia Gusev et al. (2006)	3L, 1 tile, 1E SV: Ecoclimap

ACPD
13, 18581–18620, 2013

Table 3. τ_1 and τ_2, in days, used for the exponential decay of EF after a rainfall.

site	τ_1	τ_2
ML-Grassland Bare	2.9 ± 0.3	1 ± 0.01
ML-Grassland Vegetated	6.7 ± 1	4 ± 0.2
NG-Fallow Bare	1.3 ± 0.05	1 ± 0.01
NG-Fallow Vegetated	21 ± 3.8	5.5 ± 1.4
NG-Millet Bare	2.1 ± 0.2	0.9 ± 0.04
NG-Millet Vegetated	9.9 ± 0.6	1.7 ± 0.3
BN-Fallow Vegetated	10.5 ± 1.3	1.7 ± 0.01
BN-Forest Vegetated	74 ± 55	

ACPD
13, 18581–18620, 2013

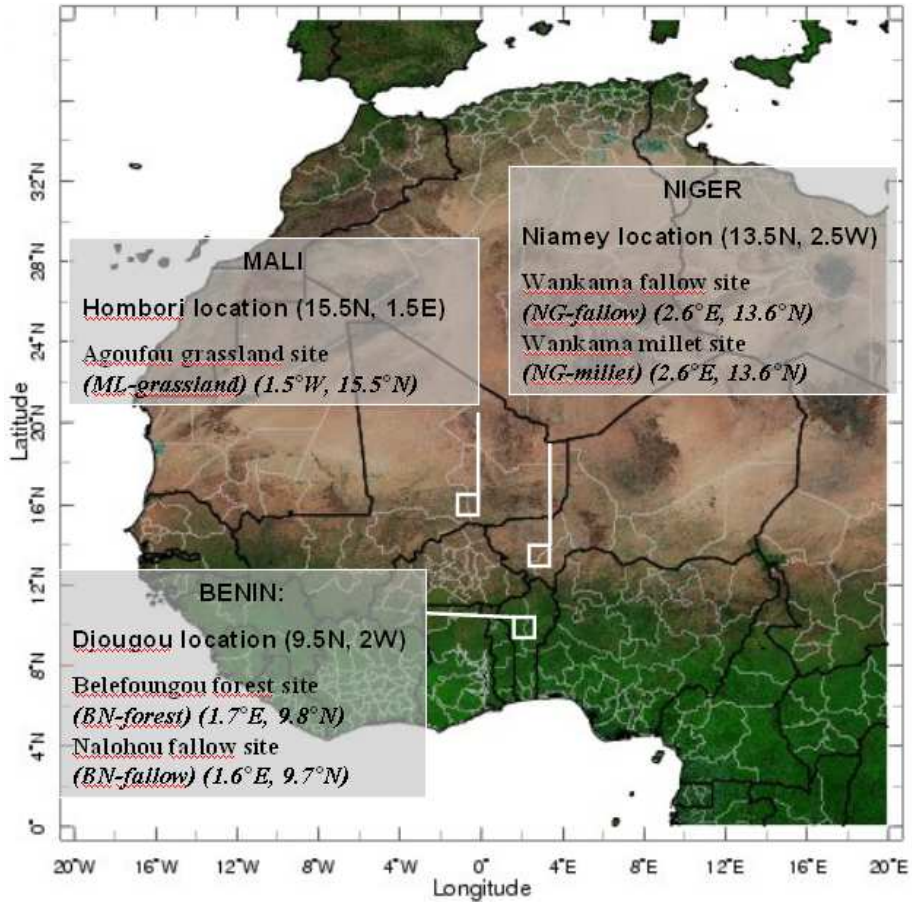

Fig. 1. Djougou (Benin), Niamey (Niger) and Hombori (Mali) gridcells containing experimental sites, where LSM data have been extracted.

ACPD
13, 18581–18620, 2013

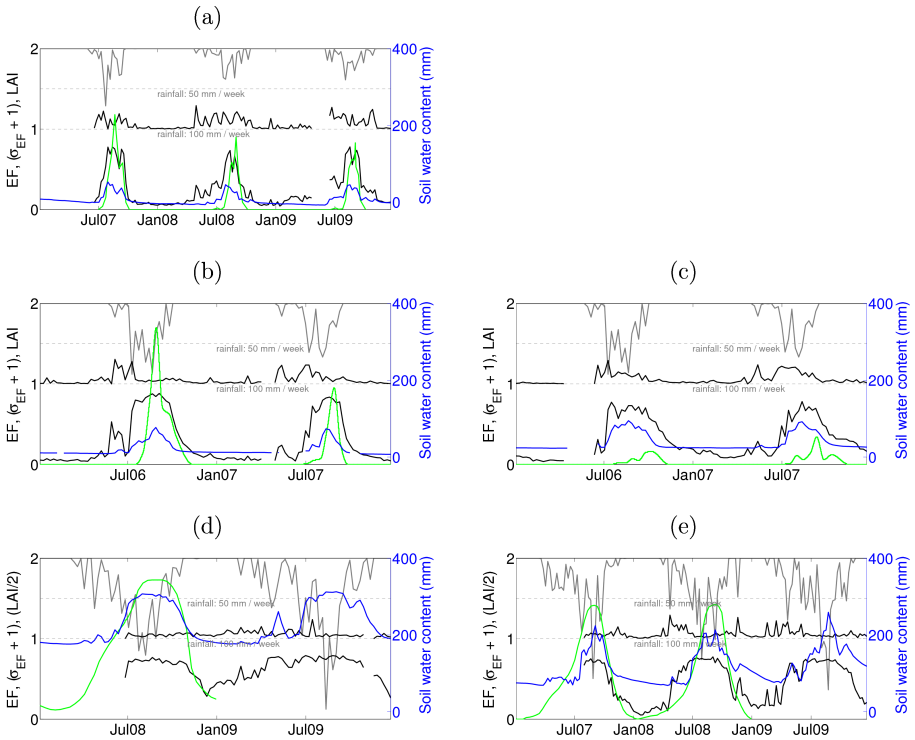

Fig. 2. Weekly (black) evaporative fraction EF and its standard deviation shifted above one (σ_{EF}), (green) LAI, (blue) soil water content and (grey) weekly rainfall (with an inverted y-axis) measured at **(a)** ML-grassland, **(b)** NG-fallow, **(c)** NG-millet, **(d)** BN-forest, **(e)** BN-fallow.

ACPD
13, 18581–18620, 2013

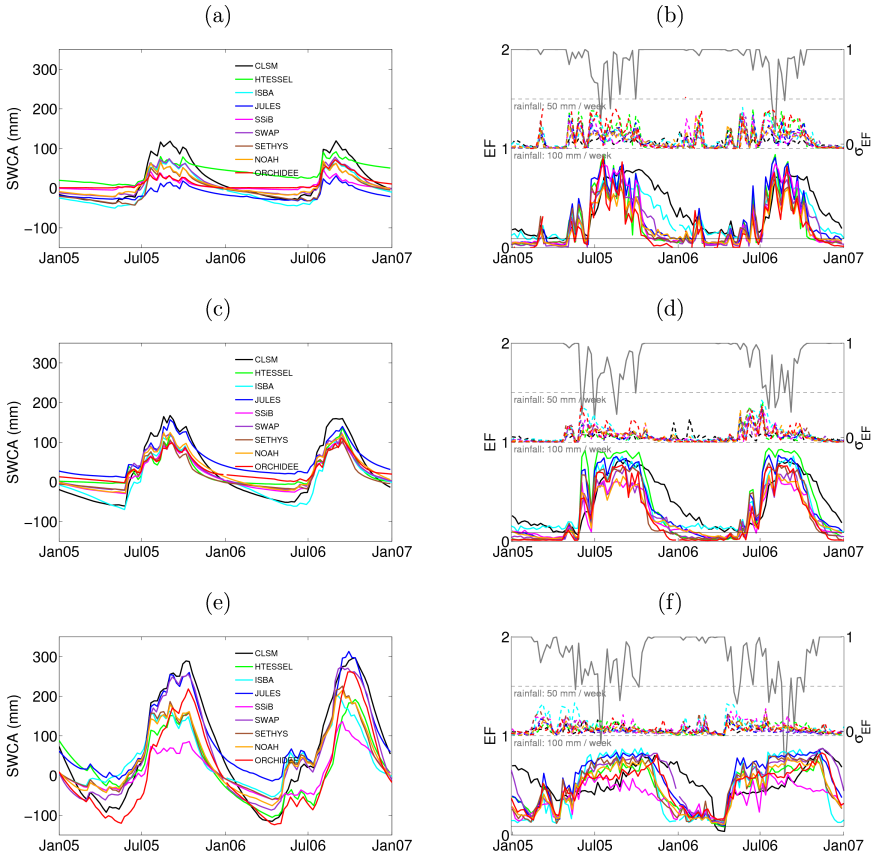

Fig. 3. Weekly (left panels) soil water content anomaly (SWCA) and (right panels, continuous colored lines) evaporative fraction EF and (dashed colored lines) its standard deviation (σ_{EF}) from january 2005 to December 2006 at **(a, b)** Hombori, **(c, d)** Niamey and **(e, f)** Djougou locations. Colors stand for the 9 LSM. Weekly rain amount (grey, with in inverted y-axis), which is one of the atmospheric forcings, is overplotted on the right panels.

ACPD
13, 18581–18620, 2013

Surface response to rain events throughout the West African monsoon

F. Lohou et al.

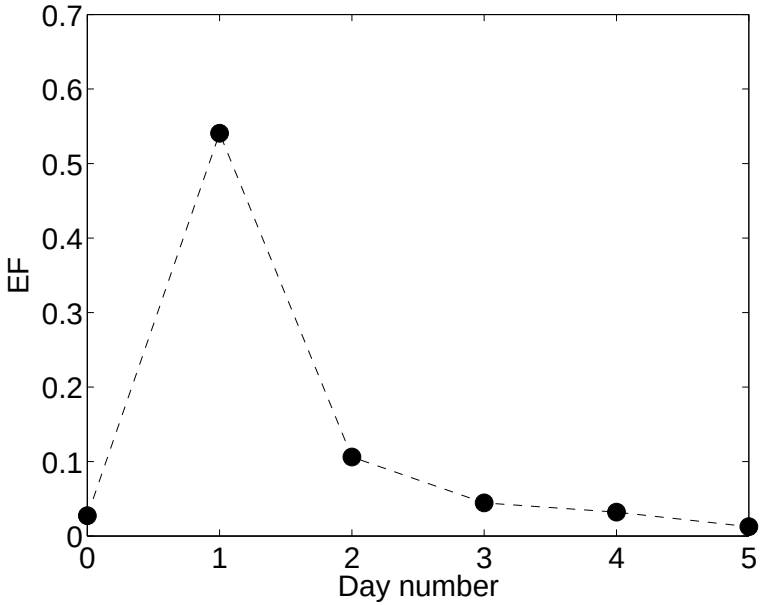

Fig. 4. Example of mean evaporative fraction evolution (EF) before (*D*0) and after (*D*1 to *D*5) a rainfall which occurred at NG-fallow at the beginnning of the monsoon.

ACPD
13, 18581–18620, 2013

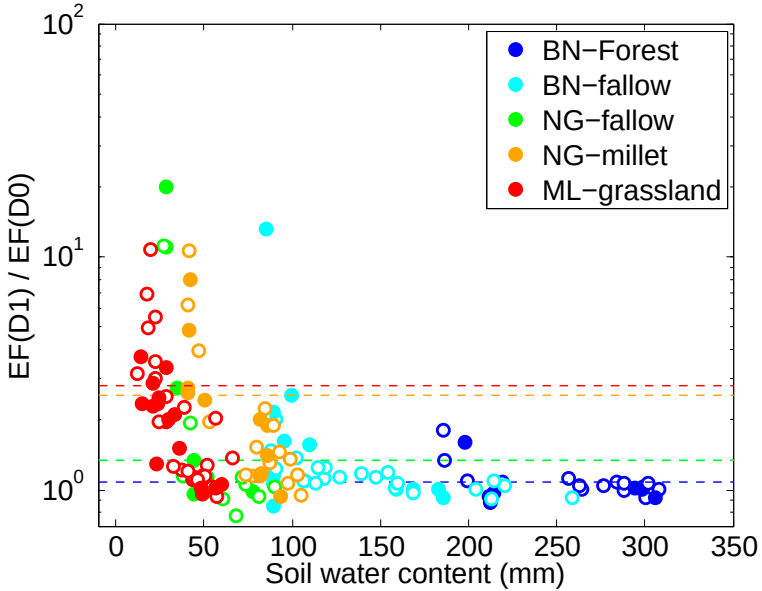

Fig. 5. Immediate surface response (EF($D1$)/EF($D0$)) against vertically integrated soil water content at $D0$. Horizontal dashed lines indicate EF($D1$)/EF($D0$) upper quartile. Colors stand for the different sites; open and full circles are respectively for cumulated rainfall ≤ 8 mm and > 8 mm.

ACPD
13, 18581–18620, 2013

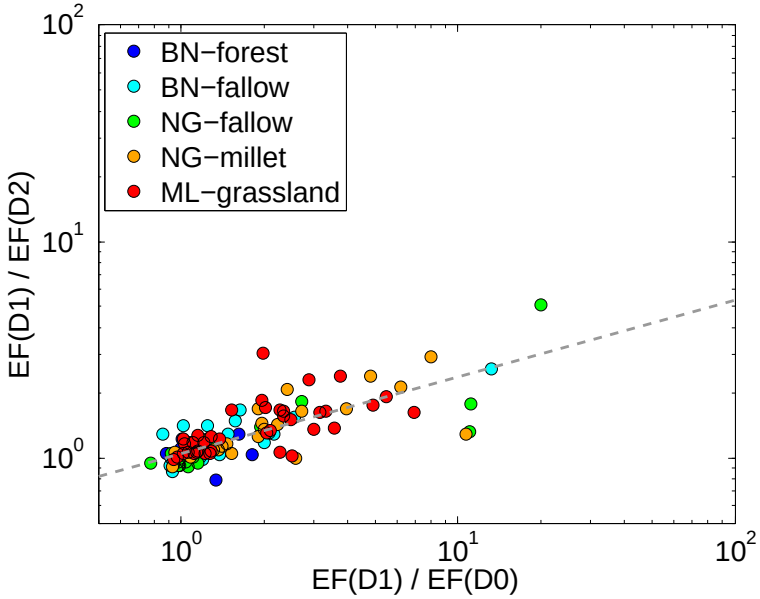

Fig. 6. Immediate surface response (EF($D1$)/EF($D0$)) against EF($D1$)/EF($D2$). Colors stand for the different sites.

ACPD
13, 18581–18620, 2013

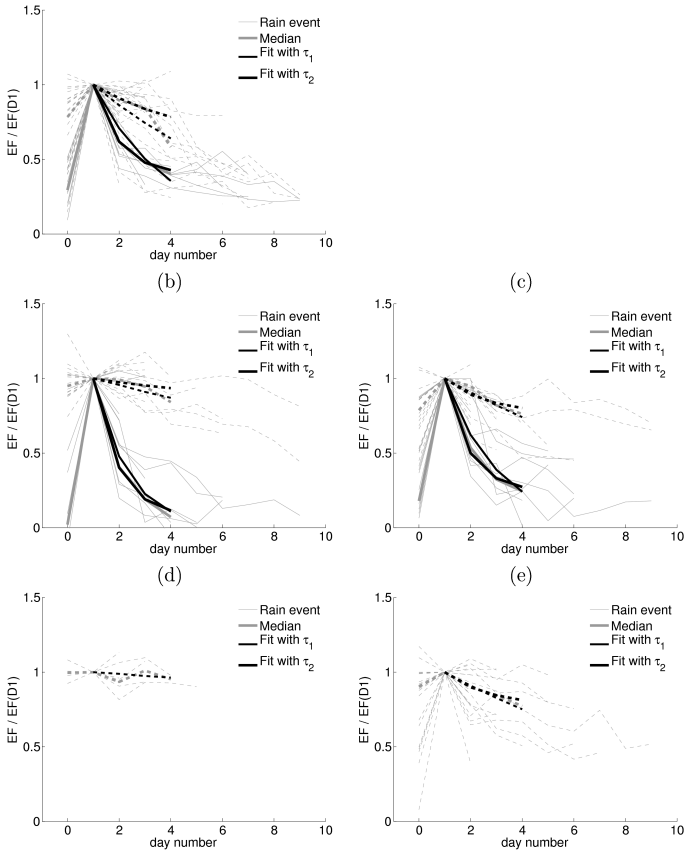

Fig. 7. Evolution of the daily normalized evaporative fraction (EF/EF($D1$)) before and after rain event for **(a)** ML-grassland, **(b)** NG-fallow, **(c)** NG-millet, **(d)** BN-forest **(e)** BN-fallow. Thin and bold grey lines stand for individual rain events and their median, respectively. Thin and bold dark lines stand for exponential fit with τ_1 and τ_2, respectively. Rain are sorted in two categories: (continuous line) bare soil (LAI $\leq$ 0.01) and (dashed line) vegetation cover (LAI $>$ 0.01).

ACPD
13, 18581–18620, 2013

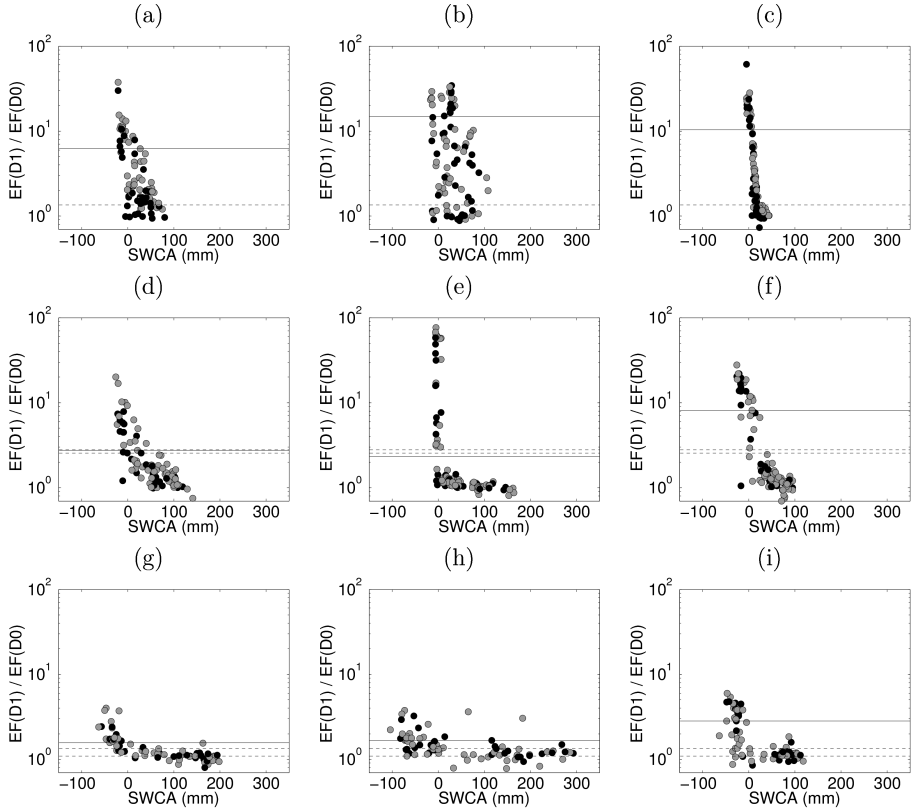

Fig. 8. Exemple of surface immediate response (EF($D1$)/EF($D0$)) against soil water content anomaly (SWCA) just before the rain, for (**a** to **c**) Hombori, (**d** to **f**) Niamey, and, (**g** to **i**) Djougou locations with 3 of the 9 LSMs involved in ALMIP (left, middle and right panels are for NOAH, HTESSEL and SSiB, respectively). Grey and dark circles are for cumulated rainfall $\leq$ 8 mm and $>$ 8 mm, respectively. Horizontal dashed and continuous lines stand for EF($D1$)/EF($D0$) upper quartile in the experiment and simulation, respectively.

ACPD
13, 18581–18620, 2013

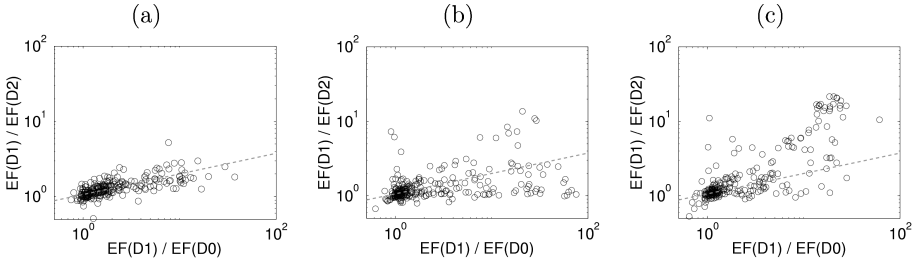

Fig. 9. Immediate surface response (EF($D1$)/EF($D0$)) against EF($D1$)/EF($D2$) simulated by 3 LSMs (**a** NOAH, **b** HTESSEL and **c** SSiB) at the three locations. The dashed line stands for the experimental relationship (Fig. 6).

ACPD
13, 18581–18620, 2013

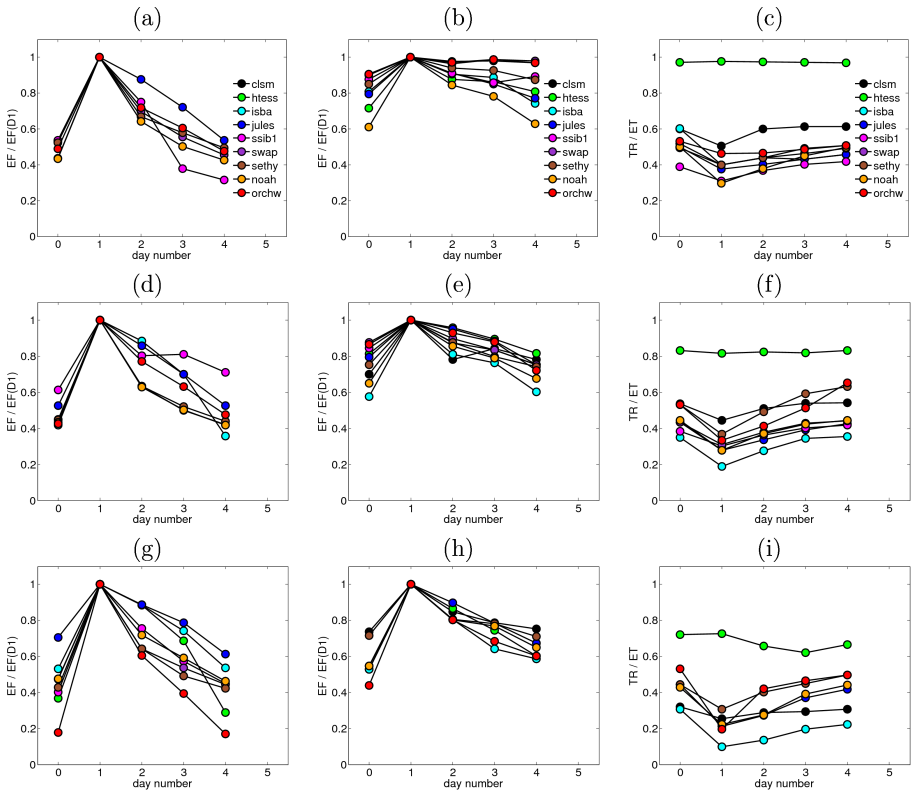

Fig. 10. Median evolution of normalised evaporative fraction (left panels) over bare soil, (middle panels) over vegetated surface and (right panels) median evolution of transpiration to evapotranspiration ratio (TR / ET) over vegetated surface from day 0 to day 4 in (**a** to **c**) Hombori, (**d** to **f**) Niamey and (**g** to **i**) Djougou. The colors stand for the 9 LSMs.

ACPD
13, 18581–18620, 2013

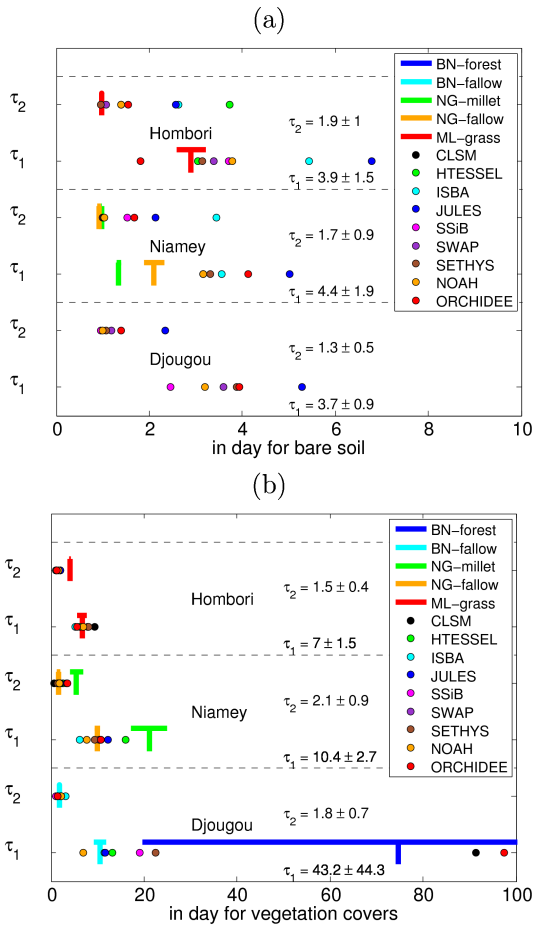

Fig. 11. τ_1 and τ_2 for experimental and simulated data at the three locations for **(a)** bare soil and **(b)** vegetation covers. Horizontal lines for the experimental values indicate the accuracy of τ estimate. Mean and standard deviation of τ estimated by LSM are indicated for each site.

ACPD
13, 18581–18620, 2013